

Searching for an additional high-energy component in Fermi-LAT GRB afterglows

Xin-Bo He, Pak-Hin Thomas Tam, Guang-Bo Long, Partha Sarathi Pal, Yong Zhang, and Li-Jun Zhang

School of Physics and Astronomy, Sun Yat-sen University, Zhuhai 519082, P. R. China,
e-mail: tanbxuan@mail.sysu.edu.cn, zhangyong5@mail.sysu.edu.cn

Received XXX; accepted XXX

ABSTRACT

Context. The very high-energy (VHE; ≥ 100 GeV) component from at least two gamma-ray bursts (GRBs), i.e., GRB 180720B and GRB 190114C, has been detected in the afterglow phase. It is widely discussed that the GeV to TeV emission is originated from synchrotron self-Compton (SSC) process. The VHE component may cause an upturn at the high-energy spectral ends in the Fermi-Large Area Telescope (Fermi-LAT) observing band.

Aims. We aim to find out whether an additional high-energy component commonly exists in the afterglows of Fermi-LAT GRBs. This study will help us to better understand how common it is for a GRB afterglow detected by Fermi-LAT to involve a VHE component.

Methods. First, we selected those GRBs that emit ≥ 10 GeV photons. The ≥ 10 GeV photons can be considered as a plausible proxy for a VHE component. We systematically analyzed 199 GRBs detected by Fermi-LAT during 2008–2019. If an additional high-energy component exists in the afterglows of Fermi-LAT GRBs, the best-fit spectral model could be a broken power-law (BPL) model with an upturn above a break energy. We compare the afterglow spectra using power-law (PL) and BPL representations.

Results. Out of the 30 GRBs with ≥ 10 GeV photons that arrived after T_{90} (the time duration when 90% of the prompt emission was detected), 25 GRBs are tentatively or significantly detected at 0.1–200 GeV after $2 \times T_{90}$. The spectrum of GRB 131231A shows an upturn above an energy break of 1.6 ± 0.8 GeV, supporting the BPL model. For GRB 131231A, we performed a modeling of its X-ray and γ -ray spectra, and found that the SSC model can explain the upturn with acceptable parameter values. In the cases of GRB 190114C, GRB 171210A, GRB 150902A, GRB 130907A, GRB 130427A, and GRB 090902B, the improvement of the BPL fit compared to the PL fit is tentative or marginal.

Conclusions. There is no conclusive evidence that an additional higher energy component commonly exists in Fermi-LAT GRB afterglows, except for a group of Fermi-LAT GRBs mentioned above. Such an additional high-energy component may be explained by the synchrotron self-Compton mechanism. Current and future VHE observations will provide important constraints on the issue.

Key words. gamma-ray bursts; radiative mechanisms

1. Introduction

Gamma-ray bursts (GRBs) consist of short (tens of milliseconds to thousands of seconds) and bright prompt emission at \sim keV to MeV energies (e.g., Rees & Mészáros 1992; Mészáros & Rees 1997), followed by longer (days to months) afterglow phase at the frequency range from radio to GeV γ -rays (e.g., Costa *et al.* 1997). Generally, the prompt emission is expected to be produced by some internal dissipation mechanisms such as collisionless shock in jet (Rees & Mészáros 1994), and the afterglow emission, from radio up to X-rays, can be described by synchrotron emission of external shock with surrounding medium (Mészáros & Rees 1997).

*Fermi Gamma-ray space Telescope*¹ (Ackermann *et al.* 2012), launched in 2008, plays an important role in the detection, as well as the spectral and timing characterisation of GRBs, with its two onboard instruments: the Large Area Telescope (LAT, 20 MeV to >300 GeV) (Atwood *et al.* 2009) and Gamma-ray Burst Monitor (GBM, 8 keV to 40 MeV) (Meegan *et al.* 2009). At >30 MeV, the Fermi-LAT can monitor GRBs in both the prompt and afterglow phases. It has detected 186 GRBs in the first decade at 100 MeV energies (see, e.g. Ajello *et al.* 2019); this corresponds to 8% of all GRBs that are detected with GBM. Photons of ≥ 10 GeV have been detected from GRBs 080916C (Abdo *et al.* 2009a), 090902B (Abdo *et al.* 2009b; Panaitescu 2017), 090328 (Panaitescu 2017), 090926A (Swenson *et al.* 2010; Ackermann *et al.* 2011; Yassine *et al.* 2017), 100414 (Panaitescu 2017), 110721 (Axelsson *et al.* 2012; Panaitescu 2017), 110731 (Ackermann *et al.* 2013b; Panaitescu 2017), 130427A (Tam *et al.* 2013; Ackermann *et al.* 2014), 130907A (Tang *et al.* 2014), 131231A (Liu *et al.* 2014), 140619B (Ruffini & Muccino 2015; Panaitescu 2017), and 160509A (Laskar *et al.* 2016; Tam *et al.* 2017).

Furthermore, Cherenkov telescope arrays MAGIC and H.E.S.S. have recently detected very high-energy (VHE; ≥ 100 GeV) emission from several GRBs, largely at the afterglow phase: GRB 180720B (Abdalla *et al.* 2019), GRB 190114C (MAGIC Collaboration *et al.* 2019a), and GRB 190829A (H.E.S.S. collaboration 2019)). In the case of GRB 190114C, the highest observed photon energy reach ~ 1 TeV (MAGIC Collaboration *et al.* 2019a).

¹ <https://fermi.gsfc.nasa.gov>

Concerning the origin of the afterglow GeV emission, synchrotron emission from external shock electrons becomes the ‘standard’ radiation mechanism in the Fermi era but there exists a maximum synchrotron energy, typically $\lesssim 10$ GeV (e.g., Kumar & Barniol Duran 2010; Piran & Nakar 2010). It is a great challenge for the traditional synchrotron mechanism to explain the $\gtrsim 10$ GeV emission, since the flux emitted by this mechanism above several GeV (the maximal cutoff energy) should be very small. The synchrotron self-Compton (SSC) component is expected to dominate in the GeV-TeV energy range (Mészáros & Rees 2000; Sari & Esin 2001; Zhang & Mészáros 2001), implying that the spectra of such GRBs should have two peaks in the broad-band spectral energy distribution (SED): one at the X-ray band, and the other at the TeV γ -ray band. Prompted by the recent VHE detections of GRBs, attempts to explain the VHE emission by the Compton processes have been performed (e.g., Wang *et al.* 2019; Fraija *et al.* 2019; Zhang *et al.* 2020).

Generally, the best-fit spectral model of LAT afterglow spectra is usually a power-law model (e.g., Ajello *et al.* 2019). Tam *et al.* (2013) was able to identify an additional hard component in the LAT afterglow in GRB 130427A. Following this, Panaitescu (2017) found a sample of LAT GRBs whose afterglow spectrum is better described by a broken power-law (BPL) with a smaller high-energy photon index (β) than low-energy photon index (α), providing a strong evidence of hardening spectrum above a few GeV. This indicates that an inverse Compton spectral component may exist in the GRB afterglow phase, and in particular in the Fermi-LAT energy band. It should be noted that the analysis by Panaitescu (2017) is based on aperture photometry, and is focused on the first 1000s after the burst onsets.

Given the detection of VHE photons by Cherenkov telescope arrays from GRB afterglows up to a day, it is desirable to look for photons with the highest energies accessible to Fermi-LAT, e.g., 10–200 GeV, up to one day post-burst. Indeed, Fermi-LAT covers the spectral range between the two peaks (synchrotron and inverse-Compton) expected in the afterglow spectra, and has likely been seen in GRB 190114C (MAGIC Collaboration *et al.* 2019b). In this work, we expand the above works to all LAT-detected GRBs, and up to one day after the burst, using maximum likelihood analysis.

2. Datasets and methods

2.1. A Search of ≥ 10 GeV photons

From 2008 to 2020, Fermi-LAT has detected more than 200 GRBs. The information about the Fermi-LAT GRBs can be obtained from the second Fermi-LAT GRB catalog (Ajello *et al.* 2019) and the Fermi website². In June 2019, Fermi-LAT team released the Second Fermi-LAT GRB Catalog (the first decade of GRBs detected by the Fermi-LAT), containing 186 LAT GRBs, from a search of a total of 2357 GRBs (Ajello *et al.* 2019). In order to enlarge the sample size of possible GRBs with high-energy photons as much as possible, we also consider GRBs listed in the webpage of Fermi LAT GRBs³. It contains 146 GRBs (including some GRBs in the second Fermi-LAT GRB Catalog). GRB 190114C is the first GRB identified to emit \sim TeV emission, so it is also included. In the end, the GRB sample considered in this work contains a total of 199 GRBs.

Fermi-LAT data were downloaded from the *Fermi-LAT database*⁴, the “extended”-class events files were downloaded which include all event classes (including the TRANSIENT class needed for GRB prompt emission analysis) and provide additional information for each event. Fermi Science Tools version 1.2.1 was used to reduce and analyze the 0.1-200 GeV data. For the event class, we chose “P8R3_Transient” if the time interval contains the prompt phase, while “P8R3_Source” was selected for the afterglow-only analysis. The zenith angle is constrained to be smaller than 100 degrees to exclude the gamma-ray emission from the Earth albedo.

In our analysis, the *gtselect* tool was used for selection cuts on the event data file. The photon class was selected with 16 for “transient” events and 128 for “source” events above 100 MeV. The search region has a radius of 10 degrees and is centred on the GRB location. The tool *gtmktime* was used to create good time intervals (GTIs) based on selections made using the spacecraft data file variables, and two tools were used to generate exposure maps: *gtlcube*, creating a livetime cube, and *gtexmap*, generating an exposure map based on the event selection imposed on the photon file and the livetime cube. To suppress the background, the two diffuse emission components *gll_iem_v07.fits*⁵ (Galactic diffuse emission) and *iso_P8R3_SOURCE_V2_v1.tx*⁶ (isotropic diffuse component) were used in our analysis, and sources in the Fermi catalog (4FGL) were included as background sources. Finally, we performed the likelihood fit using the *gtlike* tool. All spectra were analyzed as such.

Generally, the best-fit spectral model of LAT afterglow spectra is a power law (see, e.g., Ajello *et al.* 2019):

$$\frac{dN}{dE} = N_0 \left(\frac{E}{E_0} \right)^{-\Gamma}, \quad (1)$$

where N_0 is the normalisation factor, E_0 is the pivot photon energy, and Γ is the photon index. The significance of a source can be measured by the test-statistic (TS) value (Ajello *et al.* 2019), which is defined as:

$$TS = -2 \log \frac{\mathcal{L}_{\text{null}}}{\mathcal{L}_{\text{source}}}, \quad (2)$$

where $\mathcal{L}_{\text{null}}$ is the maximum of the likelihood function for the null hypothesis, and $\mathcal{L}_{\text{source}}$ is the maximum of the likelihood function for the alternative hypothesis. The detection significance of a source is around $\sim (TS)^{1/2}$ standard deviation (or σ). The goodness

² https://fermi.gsfc.nasa.gov/ssc/observations/types/grbs/lat_grbs

³ https://fermi.gsfc.nasa.gov/ssc/observations/types/grbs/lat_grbs/table.php, retrieved on 2019 March 31

⁴ <https://fermi.gsfc.nasa.gov/ssc/data/access/>

⁵ https://fermi.gsfc.nasa.gov/ssc/data/analysis/software/aux/4fgl/gll_iem_v07.fits

⁶ https://fermi.gsfc.nasa.gov/ssc/data/analysis/software/aux/iso_P8R3_SOURCE_V3_v1.txt

of the different models can be estimated through ΔTS , which is defined as: $\Delta TS_{model1-model2} = TS_{model1} - TS_{model2} = (-2\log(\mathcal{L}_{null} / \mathcal{L}_{model1})) - (-2\log(\mathcal{L}_{null} / \mathcal{L}_{model2})) = 2\log(\mathcal{L}_{model1} / \mathcal{L}_{model2})$, and the significance of improvements is calculated by $\sim (\Delta TS)^{1/2}$ standard deviation (or σ).

To search for ≥ 10 GeV photons, we analyzed all 199 GRBs with the time interval from the burst onset to 1 day thereafter with the steps described above⁷. Following that, we used the *gtsrcprob*⁸ tool to estimate the probability of each photon coming from a GRB, P_{source} . We check all the 199 GRBs to look for ≥ 10 GeV photons associated with a GRB, which are those with $P_{GRB} \geq 97\%$. Finally, we obtain 67 photons above 10 GeV from 34 GRBs. The properties of these 67 photons and some properties of the 34 GRBs are given in Tables 1–3.

These 34 GRBs are potential GRBs associated with very high-energy photons. Our samples include the 29 GRBs discovered by Fermi-LAT collaboration (Ajello *et al.* 2019) with >10 GeV photons detected, so our results are consistent with the analysis of the Fermi-LAT collaboration (Ajello *et al.* 2019). Among the 34 GRBs, only one GRB (GRB 090510A) is short-duration, and the others are long GRBs. According to when the > 10 GeV photons arrived relative to the GRB trigger time, three categories can be seen:

- for 27 GRBs, the ≥ 10 GeV photons arrived after T_{90} (T_{90} is the time duration when 90% of the prompt emission was detected, see Table 1);
- for GRBs 160625B, 140619B, 110903A, 080916C, their ≥ 10 GeV photons arrived in T_{90} (see Table 2);
- for GRBs 160509A, 130427A, 090902B, ≥ 10 GeV photons arrived in T_{90} and after T_{90} (see Table 3).

All photons have energy below 100 GeV (in the observer’s frame), except for an interesting event – a 173 GeV photon arrived at 57071 s after trigger with about 97% probability being associated with GRB 131231A. The energy and arrival time of these photons in observer’s and source frames (when a measured redshift is available) are displayed in Figure 1.

It is clear that most ≥ 10 GeV photons arrived in the afterglow phase, except for GRBs 160625B, 140619B, 110903A, 080916C. It is rather non-trivial to explain late time ≥ 10 GeV photons by synchrotron emission from external shock, as the maximum (cutoff) photon energy radiated by synchrotron is ~ 5 GeV (Piran & Nakar 2010; Abdo *et al.* 2009a; Barniol Duran & Kumar 2011), while an additional component in afterglow phase could explain ≥ 10 GeV photons. It is therefore desirable to see if an additional high-energy spectral component can exist in the Fermi-LAT spectra, especially at the high energy end above 10 GeV. We now turn to the analysis of the 30 Fermi-LAT afterglow spectra.

2.2. Spectral analysis of significantly LAT-detected GRB afterglows with ≥ 10 GeV photons

To systematically analyze these 30 GRB afterglows, we adopt a unified end time (86.4 ks post-burst). The analyze time intervals start at $2 \times T_{90}$ and end at ~ 86.4 ks for every GRB, where $2 \times T_{90}$ is adopted to minimise the contamination of the prompt emission at GeV energies. The reasons to derive time-integrated spectra instead of time-resolved ones are two-fold: (1) the number of photons for many of the LAT GRBs especially in the afterglow phase is small; (2) there is no strong indication for change of spectral index during the afterglow phase (Ackermann *et al.* 2013a).

Out of the 30 GRBs with ≥ 10 GeV photons arrived after T_{90} , 25 GRBs are tentatively or significantly detected after $2 \times T_{90}$ with $TS \geq 4$, and this sample will form a basis to study the GeV afterglow spectra as a population.

We first use the power-law (PL) model to describe the observed spectra. To compare the photon spectral indices between the 25 GRBs with the other 174 LAT GRBs, we plot the index distribution in Figure 2. The average spectral index of these 25 GRBs ($\Gamma = 1.83 \pm 0.53$) is comparable to that of the typical Fermi-LAT GRBs ($\Gamma = 1.69 \pm 0.28$). We found that the power-law index distribution for the two populations is indeed similar, which indicates that there may not be intrinsic difference between the GeV spectra of the two groups.

To search for an additional higher energy component in these 25 Fermi-LAT GRB afterglows, We utilize the broken power-law (BPL) model to describe these GRBs, following Tam *et al.* (2013) and Panaitescu (2017). BPL model may improve the fitting if an additional hard component exists in the spectrum. Subsequently, we consider the BPL model for the 25 GRBs:

$$\frac{dN}{dE} = N_0 \begin{cases} \left(\frac{E}{E_b}\right)^{-\alpha} & \text{if } E < E_b, \\ \left(\frac{E}{E_b}\right)^{-\beta} & \text{if } E \geq E_b, \end{cases} \quad (3)$$

where E_b is the break energy.

2.3. The possible additional higher energy components in the afterglow spectra

To identify the most probable GRBs in which an additional higher energy component may exist in the afterglow. We compare the afterglow spectra using power-law and broken power-law (BPL) representations. There are 18 GRBs that can be well fit by the PL and BPL models. In Figures 3 and 4, we plot the SEDs including the butterfly plots and spectral points. The PL and BPL parameters of the 18 GRBs are shown in Tables 4 and 5. In the cases of GRB 100213C, GRB 101014A, GRB 120916A, GRB 130502B, GRB 160422A, GRB 160521B, and GRB 160509A, small values of the break energy, E_{break} , do not allow the low-energy index (i.e., α) to be well constrained in the BPL fits.

⁷ we do not restrict ourselves to the time frame $\geq T_{90} \times 2$ to archive a complete search of ≥ 10 GeV photons from LAT GRBs.

⁸ this tool assigns a probability of each photon event that it belongs to a particular source, c.f., <https://raw.githubusercontent.com/fermi-lat/fermitools-fhelp/master/gtsrcprob.txt>

To search for candidates for which a BPL fits better than a PL, we impose a criterion on the 0.1–200 GeV GRB spectra: based on the butterfly plots, the BPL model should have improvement over the PL model with $\Delta TS_{BPL-PL} > 3$, and in the BPL model, the high-energy index (β) is harder than the low-energy index (α), and the spectral points SEDs also show the same behavior that a possible upturn exists in the higher energy. Three categories are drawn:

- for GRB 131231A, ΔTS_{BPL-PL} is 13.63 ($\sim 3.7\sigma$), and an upturn exists above the E_{break} . Therefore the BPL model is significantly preferred over the PL model;
- for GRB 190114C, 171210A, 150902A, 130907A, 130427A, and 090902B, they all satisfy $\Delta TS_{BPL-PL} > 3$ and show a possible upturn above the E_{break} , therefore the improvements should be tentative or marginal;
- for the GRBs with $\Delta TS_{BPL-PL} < 3$, there is no preference for any model.

We also plot the spectra of the 7 GRBs ($\Delta TS_{BPL-PL} > 3$) in Figure 5, and the break energy E_b is around 1 GeV for many of these spectra.

For the above 7 GRBs with $\Delta TS_{BPL-PL} > 3$, if the additional high energy component exists, it could originate from SSC. In this case, the index (β) of the high energy component should be harder than the index (α) of synchrotron emission at lower energies, the spectrum can be well fit by a BPL model with $\alpha - \beta = 0.5$ (e.g., Panaitescu 2017). Therefore, we define BPL $_{\alpha-\beta=0.5}$ model with $\alpha - \beta$ fixed at 0.5 to describe the SSC spectrum. We find all 7 GRBs could be fit by BPL $_{\alpha-\beta=0.5}$ model. It supports that an SSC-like spectrum is acceptable for these 7 cases. The fit results are presented in Table 4.

To summarise, we found that the BPL improvement for GRB 131231A is significant, with a maximum $\Delta TS_{BPL-PL} = 13.63$ ($\sim 3.7\sigma$) and an upturn above $E_{break} = 1.6 \pm 0.8$ GeV. For GRB 190114C, GRB 171210A, GRB 150902A, GRB 130907A, GRB 130427A, and GRB 090902B, we regard the improvement of the BPL fit over PL to be tentative or marginal, since these 6 GRBs show $\Delta TS_{BPL-PL} > 3$ and a possible upturn above E_{break} . The spectra of the other GRBs can be fitted equally well by the two models.

2.4. The possible additional higher energy components in the prompt spectra

For these 7 GRBs, it is desirable to see whether the additional high energy component exists in prompt emission as well. For that, we check whether the spectrum exhibits an upturn during the prompt phase or shortly after. Therefore, we ran the unbinned analysis chain in T_0 to $T_0 + 2 \times T_{90}$ (where T_0 is the GRB onset time) to get a power-per-decade spectra F , defined as

$$F = E \frac{dN}{dE} \propto (E)^{-\gamma}. \quad (4)$$

Only GRB 090902B, GRB 130427A and GRB 190114C show significant prompt emission. For these 3 GRBs, the high enough number of photons allow us to plot bin-wise spectra. The power-per-decade spectra F of these three GRBs are shown in Figure 6. We use the PL and BPL models to fit the data points with linear regression, and the $\chi^2/d.o.f.$ values show that the BPL model gives a better fit for GRB 130427A than the PL model does. It is also apparent that an upturn exists in GRB 130427A during the prompt phase (i.e., T_0 to $T_0 + 2 \times T_{90}$), and the break energy is ~ 2 GeV. In the prompt phase of GRB 190114C, the time-resolved spectrum shows that the spectrum evolves from a BPL to a PL over the course of the prompt phase (Ajello *et al.* 2020; Vikas *et al.* 2020). In our analysis, we used time-integrated spectra over the whole prompt phase, and both models can describe the spectrum equally well.

3. Discussion

We found a group of GRB afterglows where an additional high energy component above ~ 1 GeV may exist (see Figure 3). By comparing the TS values of these 7 GRBs assuming either the PL or the BPL model, we found that the BPL model is the preferred model for GRB 131231A, as in this case $\Delta TS_{BPL-PL} = 13.63$ ($\sim 3.7\sigma$) is found, supported by an upturn above the E_{break} . We found tentative (or marginal) evidence that the BPL model could be superior to the PL model ($3 < \Delta TS_{BPL-PL} < 9$ and a possible upturn above E_{break}) for the cases GRB 190114C, GRB 171210A, GRB 150902A, GRB 130907A, GRB 130427A, and GRB 090902B. One should note that, as time evolves in the afterglow phase, the break energy could vary or even move outside of the instrument energy range, smoothing any sharp upturn when summing over spectra at different times. Therefore, evidence of such an upturn in *time-integrated* afterglow spectra could strengthen the existence of an upturn.

It is hard to explain the late-time ≥ 10 GeV photons by synchrotron emission (which is typically used to explain afterglow emission below ~ 1 GeV), and the evidence of an upturn above a break energy of ~ 1 GeV requires an additional spectral component at high energy. A leading explanation for this additional component is the SSC radiation in the external forward shock (see, e.g., MAGIC Collaboration *et al.* 2019b, for the case of GRB 190114C). It has been predicted over the past two decades (Panaitescu & Mészáros 1998; Wei & Lu 1998; Sari & Esin 2001; Zhang & Mészáros 2001; Mészáros *et al.* 2004; Fan & Piran 2008; Galli & Piro 2008; Nakar *et al.* 2009; Piran & Nakar 2010; Lemoine 2015) and the VHE afterglow emission detected in GRB 180720B and GRB 190114C provides a strong evidence for such an SSC component origin (MAGIC Collaboration *et al.* 2019b; Abdalla *et al.* 2019).

If the additional component is caused by SSC, in the synchrotron-SSC scenario, the Fermi-LAT spectrum below E_b representing the synchrotron emission would have a photon index larger than 2, while the SSC emission starts to dominate above a few GeV making the spectra “anomalously” turn up above the break energy. This is broadly consistent with the 7 GRBs with an upturn at ~ 1 GeV.

In order to investigate whether the SSC emission can explain the new component, we fit the observations of GRB 131231A whose spectrum upturn is the most significant in terms of ΔTS_{BPL-PL} with a simple SSC model presented by Sari *et al.* (1998) and Sari & Esin (2001). This model gives an analytic approximation of synchrotron and SSC spectra ignoring the Klein-Nishina effects. This approximation is adequate given the limited photon statistics up to 200 GeV. The result of modeling to the Swift XRT and Fermi-LAT data of GRB 131231A, within the framework of the theory of afterglow emission from external forward shocks (Sari *et al.* 1998; Sari & Esin 2001), is shown in Figure 7. The Swift-XRT data are analyzed by HEASOFTv6.25. The X-ray spectra are fitted with an absorbed, redshifted power-law model considering the column density of the Galactic hydrogen of $n_H = 0.028 \times 10^{22} \text{ cm}^{-2}$, that of the intrinsic hydrogen of $n_H = 0.24 \times 10^{22} \text{ cm}^{-2}$, and a redshift of $z = 0.642^9$. The X-ray spectral index is obtained as $\Gamma = 2.76_{-1.61}^{+1.52}$, which gives an unabsorbed 0.3–10.0 keV flux of $(2.09 \pm 0.9) \times 10^{-13} \text{ erg cm}^{-2} \text{ s}^{-1}$.

We found that the SSC model can explain the upturn of the Fermi-LAT observed spectrum if the conditions at the source are the following. The energy of the spherical shock is roughly estimated to be $E \approx 9.2 \times 10^{52} \text{ erg}$ through the observed energy fluence ($\approx 3.7 \times 10^{-4} \text{ erg cm}^{-2}$) from 100 MeV to 200 GeV and 60 s to 1 day after the burst onset. The relativistic shock propagates into a constant surrounding density $n \approx 1 \text{ cm}^{-3}$, accelerating the electrons and forming a power law distribution of Lorentz factor γ_e with an index $p = 2.13_{-0.05}^{+0.25}$. A constant fraction $\epsilon_e = 0.16_{-0.03}^{+0.04}$ of the shock energy goes into the electrons and about 20% of the electron energy is radiated away via the synchrotron and SSC emission. A fraction $\epsilon_B = 1_{-0.5}^{+39} \times 10^{-5}$ of the shock energy goes into amplifying the magnetic fields behind the shock. These three (n is fixed) free-parameter values of p , ϵ_e and ϵ_B are resulted from an acceptable fit with the best goodness of fit $\chi^2/\text{d.o.f.} = 4.23/(8-3)$ and their ranges correspond to one σ confidence interval.

Corresponding to these values of fitting parameters and the observed time, the emitting relativistic electrons are in the regime of slow cooling. We note that $\epsilon_e \gg \epsilon_B$, thus the necessary condition for efficient production of SSC radiation can be satisfied (Sari *et al.* 1998; Sari & Esin 2001). These results are consistent with a previous work by Liu *et al.* (2014) on the same GRB, who focus especially on the origin of the GeV afterglow before 1000s post-burst.

Based on the spectra shown in Figure 5, the spectra at high energies are harder than low energies, if both components originate from the same shock, the low energy component is synchrotron emission and higher energy components possibly are SSC emission. In this case, the synchrotron emission should be produced above the cooling break, and $\alpha = p/2$, SSC spectral index in the Fermi-LAT band should be $\beta = (p-1)/2$, such that $(\alpha-\beta) = 1/2$ (Panaitescu 2017). In our BPL results, we indeed found that $(\alpha-\beta) \sim 0.52$ for GRB 130427A and $(\alpha-\beta) \sim 0.49$ GRB 090902B, satisfying $(\alpha-\beta) = 1/2$. We also found that the BPL model with $\alpha-\beta = 0.5$ being fixed gives acceptable fits for the 7 GRBs.

We compared the spectra of these 7 GRBs above 20 GeV with the sensitivity of Cherenkov Telescope Array (CTA) and Major Atmospheric Gamma Imaging Cherenkov telescope (MAGIC) (Giuseppe 2019). We assume $z=1$ for GRB 171210A and GRB 150902A. After considering the EBL absorption (Franceschini *et al.* 2017) and performing an optimistic and extreme assumption that the spectrum extends with the same high-energy index (β) up to 10 TeV¹⁰, the result is shown in Figure 8. It can be seen that given favourable observing conditions, GRB 130427A, GRB 131231A, and GRB 190114C can likely be detected by CTA and MAGIC. The question on whether the additional component commonly exists in Fermi-LAT GRBs can be ultimately tested by a large number of GRB observations using the LHAASO-WCDA detector (Bai *et al.* 2019), CTA array (Cherenkov Telescope Array Consortium 2019) and the currently operating Cherenkov telescopes.

The photon index distribution of the 25 GRBs (with ≥ 10 GeV detected) is similar to other 174 Fermi-LAT GRBs, and both are indeed rather hard ($\Gamma < 2$) at the LAT band (see Figure 2). This result lends support to the idea that these 25 GRBs do not form a distinctive class of their own, and their LAT afterglow spectra are not dissimilar to most other Fermi-LAT GRBs.

4. Conclusions

Based on the analysis of a large sample of Fermi-LAT afterglows, there is no conclusive evidence that an additional higher energy component commonly exists in Fermi-LAT GRB afterglows. On one hand, a group of GRBs, namely, GRB 190114C, GRB 171210A, GRB 150902A, GRB 131231A, GRB 130907A, GRB 130427A, and GRB 090902B, marginally or significantly supported by the plausible existence of an upturn above the break energy in the more preferred BPL model, might require such a component at the high energy end. For GRB 130427A, the spectral upturn appears in both prompt and afterglow phases. On the other hand, the BPL model is not required in the large majority of cases, as there is no improvement of the BPL fit compared to the PL fit for all other cases.

If the additional component really exists, it may be resulted from an SSC component. Besides, we find that the SSC model can explain the upturn in GRB 131231A under acceptable typical parameter values of GRBs. Another evidence for the possible SSC component is provided by GRB 130427A and GRB 090902B whose $\alpha-\beta$ (~ 0.52 and ~ 0.49 , respectively) largely satisfy $\alpha-\beta = 0.5$, and all 7 GRBs could be satisfactorily fit by the BPL $_{\alpha-\beta=0.5}$ model. These suggest that SSC emission exists in a group of GRBs (regardless of whether they are detected by ground-based VHE telescopes), and the SSC emission may last from the prompt to afterglow phases, as seen in GRB 130427A.

The possible additional high-energy component found in a group of Fermi-LAT GRBs is clearly in contradiction with a single component such as synchrotron emission for these afterglows, and SSC emission is a widely discussed mechanism to explain the additional high-energy component. Current and future VHE observations using CTA, LHAASO, and currently operating Cherenkov telescopes will provide important constraints on whether SSC emission commonly exists among GRB afterglows.

⁹ https://www.swift.ac.uk/xrt_spectra/00020336/

¹⁰ this assumption is an extreme case, ignoring the cutoff in the natural SSC spectra slope, the Klein-Nishina effect and the pair opacity in the very high energy

Acknowledgments

This work is supported by the National Natural Science Foundation of China (NSFC) grants 11633007 and U1731136, and Guangdong Major Project of Basic and Applied Basic Research (Grant No. 2019B030302001). Y.Z. thanks NSFC grant number 11973099 for financial support. This work made use of the LAT data and science tools available at the Fermi Science Support Center.

References

- Abdalla, H., Adam, R., Aharonian, F. A. *et al.*, 2019, *Nature*, 575, 466
- Abdo, A., Ackermann, M., Arimoto, M. *et al.*, 2009b, *Science*, 323, 1688
- Abdo, A., Ackermann, M., Ajello, M. *et al.*, 2009b, *ApJ*, 706, L138
- Ackermann, M., Ajello, M., Asano, K., *et al.*, 2011, *ApJ*, 729, 114
- Ackermann, M., *et al.*, 2012, *ApJS*, 203, 4
- Ackermann, M. *et al.* (Fermi/LAT collaboration) 2013a, *ApJS*, 209, 11
- Ackermann, M., Ajello, M., Asano, K., *et al.*, 2013b, *ApJ*, 763, 71
- Ackermann, M., Ajello, M., Asano, K. *et al.*, 2014, *Science*, 343, 6166
- Axelsson, M., Baldini, L., Barbiellini, G., *et al.*, 2012, *ApJL*, 757, L31
- Ajello, M., Arimoto, M., Axelsson, M. *et al.*, 2019, *ApJ*, 878, 52
- Ajello, M., Arimoto, M., Axelsson, M. *et al.*, 2020, *ApJ*, 890, 9
- Atwood, W. B., *et al.*, 2009, *ApJ*, 697, 1071
- Bai, X., Bi, B. Y., Bi, X. J., *et al.* (The LHAASO collaboration), 2019, preprint[arXiv:1905.02773]
- Barniol Duran, R., & Kumar, P., 2011, *MNRAS*, 412, 522
- The CTA Consortium 2019 <https://www.worldscientific.com/doi/pdf/10.1142/10986>
- Costa, E. *et al.* 1997, IAU Circular No. 6572
- Fan, Y. Z., & Piran, T., 2008, *Fron. Phys. China.*, 3, 306
- Frajna, N., Barniol Duran, R., Dichiara, S., Beniamini, P., 2019, *ApJ*, 883, 162
- Franceschini, A. & Rodighiero, G., *A&A*, 603, A34
- Galli, A. & Piro, L., 2008, *A&A*, 489, 1073
- Giuseppe, Di *et al.*, 2019, *EPL Web of Conferences* 209, 01035
- The H.E.S.S. collaboration, 2019, *GCN Circ. # 25566*, <https://gcn.gsfc.nasa.gov/gcn3/25566.gcn3>
- Klebesadel, R. W., Strong, I. B., & Olson, R. A. 1973, *ApJ*, 182, L85
- Kumar, P. & Barniol Duran, R. 2010, *MNRAS*, 409, 226
- Laskar, Tanmoy; Alexander, Kate D.; Berger, Edo., *et al.*, 2016, *ApJ*, 833, 88
- Lemoine, M., 2015, *MNRAS*, 453, 3772
- Liu, B., Chen, W., Liang, Y.-F. 2014, *ApJL*, 787, L6
- MAGIC Collaboration, 2019a, *Nature*, 575, 455
- MAGIC Collaboration, 2019b, *Nature*, 575, 459
- Meegan, C. A., Paciesas, W. S., Pendleton, G. N., *et al.*, 1998, *AIP Conf. Proc.*, 428, 3
- Meegan, C. A., *et al.*, 2009, *ApJ*, 702, 791
- Mészáros, P. & Rees, M. J., 1997, *ApJ*, 476, 232
- Mészáros, P. & Rees, M. J., 2000, *ApJ*, 541, L5
- Mészáros, P., Razzaque, S., & Zhang, B., 2004, *New Astron. Rev.*, 48, 445
- Nakar, E., Ando, S., & Sari, R., 2009, *ApJ*, 703, 675
- Panaitescu, A., 2017, *ApJ*, 837, 13
- Panaitescu, A., & Mészáros, P., 1998, *ApJ*, 501, 772
- Piran, T. & Nakar, E., 2010, *ApJ*, 718, L63
- Rees, M. J. & Mészáros, P. 1992, *MNRAS*, 258, 41
- Rees, M. J. & Mészáros, P. 1994, *ApJ*, 430, L93
- Ruffini, R., Muccino, M., & Kovacevic, M. 2015, *ApJ*, 808, 190
- Sari, R., & Esin, A. A., 2001, *ApJ*, 548, 787
- Sari, R., Piran, T., & Narayan, R., 1998, *ApJ*, 497, L17
- Swenson, C., Maxham, A., Roming, P. W. A., *et al.*, 2010, *ApJL*, 718, L14
- Tam, P.-H. T., Tang, Q.-W., Hou, S.-J., *et al.*, 2013, *ApJL*, 771, L13
- Tam, P.-H. T., He, X. B., Tang, Q.-W., *et al.*, 2017, *ApJL*, 844, L2
- Tang, Q.-W., Tam, P.-H. T. & Wang, X. Y., 2014, *ApJ*, 788, 156
- Chand, V., Pal, P. S., Banerjee, A., *et al.*, 2020, *ApJ*, 903, 9
- Wang, X. Y., Liu, R. Y., Zhang, H. M., *et al.*, 2019, *ApJ*, 884, 117
- Wei, D. M., & Lu, T., 1998, *ApJ*, 505, 252
- Yassine, M., Piron, F., Mochkovitch, R. *et al.*, 2017, *A&A*, 606, 17
- Zhang, B. & Mészáros, P. 2001, *ApJ*, 559, 110
- Zhang, H., Christie, I. M., Petropoulou, M., *et al.*, 2020, *MNRAS*, 496, 974

Table 1. Highest energy events of *Fermi*-LAT GRBs for which ≥ 10 GeV photons arrive after T_{90} only

Name	GRB Properties			Photon Properties				
	$T_{90}^a_{of}$	$T_{90}^b_{sf}$	Redshift ^c	Energy ^d _{of}	Arrival time ^e _{of}	Energy ^f _{sf}	Arrival Time ^g _{sf}	P ^h
190114C	116.0	81.4	0.43	18.94	8849.2	27.0	6210.0	1
171210A	143.1	–	–	12.49	1374.6	–	–	1
171022A	13.3	–	–	13.98	4582.8	–	–	1
171010A	107.3	80.7	0.33	19.00	2891.0	25.3	2173.7	1
160623A	107.8	78.9	0.37	18.21	12039.8	24.9	8807.5	1
160521B	2.8	–	–	12.69	423.7	–	–	1
160422A	12.3	–	–	12.29	771.4	–	–	1
160310A	25.6	–	–	26.99	5886.0	–	–	1
150902A	13.6	–	–	10.59	98.9	–	–	1
140928A	17.9	–	–	51.76	2555.2	–	–	1
–	–	–	–	38.62	3100.9	–	–	1
140810A	81.7	–	–	15.38	1490.3	–	–	1
140416A	31.7	–	–	10.08	2208.3	–	–	1
140206B	27.3	–	–	10.96	6736.7	–	–	1
–	–	–	–	29.39	75494.0	–	–	1
131231A	31.2	19.0	0.64	48.29	110.4	79.3	67.2	1
–	–	–	–	17.14	844.0	28.1	514.0	1
–	–	–	–	173.17	57071.0	284.4	34757.0	0.97
130907A	115.0	51.4	1.24	50.96	17161.0	114.1	7668.0	1
130502B	24.3	–	–	31.10	222.1	–	–	1
120919B	118.0	–	–	12.70	605.0	–	–	1
120916A	53.0	–	–	21.57	13004.8	–	–	1
120526A	43.6	–	–	14.30	1354.3	–	–	1
101014A	449.4	–	–	13.60	2750.7	–	–	1
–	–	–	–	11.20	2962.0	–	–	1
100511A	42.4	–	–	46.00	161.9	–	–	1
–	–	–	–	18.00	179.8	–	–	1
100414A	26.5	11.1	1.37	29.80	34.4	70.6	14.5	1
–	–	–	–	25.13	359.5	59.5	151.8	1
100213C	60.0	–	–	34.00	3389.0	–	–	1
100116A	102.5	–	–	32.64	379.2	–	–	1
–	–	–	–	13.35	296.7	–	–	1
090926A	20.0	6.4	2.11	19.46	25.8	60.5	8.3	1
–	–	–	–	10.42	3786.0	32.4	1217.4	1
090510A	1.0	0.5	0.90	29.91	1.8	56.8	0.9	1
090427A	12.3	–	–	14.10	422.9	–	–	1

Notes. The unit of energy is GeV, T_{90} and arrival times are in seconds.

^(a,d,e) Observation Frame_{of}; ^(b,f,g) Source Frame_{sf}; ^(a^{ref}) <https://heasarc.gsfc.nasa.gov/cgi-bin/W3Browse/w3hdprods.pl>;

^(c^{ref}) <http://www.mpe.mpg.de/~jcg/grbgen.html>; ^(h) Probability of the photon being associated with that GRB.

Table 2. Events with the highest energy of *Fermi*-LAT GRBs for which ≥ 10 GeV photons arrive in T_{90} only

Name	GRB Properties			Photon Properties				
	$T_{90}^a_{of}$	$T_{90}^b_{sf}$	Redshift ^c	Energy ^d _{of}	Arrival time ^e _{of}	Energy ^f _{sf}	Arrival Time ^g _{sf}	P ^h
160625B	453.4	188.4	1.41	15.30	347.5	36.8	144.4	1
140619B	2.8	–	–	22.74	1.1	–	–	1
110903A	341.3	–	–	15.60	301.0	–	–	1
080916C	63.0	11.8	4.35	12.42	17.2	66.5	3.2	1
–	–	–	–	27.43	41.1	146.7	7.7	1

Notes. The unit of energy is GeV, T_{90} and arrival times are in seconds;

^(a,d,e) Observation Frame_{of}; ^(b,f,g) Source Frame_{sf}; ^(a^{ref}) <https://heasarc.gsfc.nasa.gov/cgi-bin/W3Browse/w3hdprods.pl>;

^(c^{ref}) <http://www.mpe.mpg.de/~jcg/grbgen.html>; ^(h) Probability of the photon being associated with that GRB.

Table 3. Events with the highest energy of *Fermi*-LAT GRBs for which ≥ 10 GeV photons arrive both within T_{90} and thereafter

Name	GRB Properties			Photon Properties				
	$T_{90}^{a,of}$	$T_{90}^{b,sf}$	Redshift ^c	Energy ^d _{of}	Arrival time ^e _{of}	Energy ^f _{sf}	Arrival Time ^g _{sf}	P ^h
160509A	369.7	170.4	1.17	51.90	55.7	112.6	25.7	1
	–	–	–	41.51	221.4	90.1	102.0	1
	–	–	–	28.90	69688.6	62.7	32114.6	1
130427A	138.2	103.1	0.34	94.12	243.6	126.1	181.8	1
	–	–	–	77.11	19.1	103.3	14.2	1
	–	–	–	57.42	256.7	76.9	191.6	1
	–	–	–	38.67	78.8	51.8	58.8	1
	–	–	–	38.19	3410.3	51.2	2545.2	1
	–	–	–	33.65	34366.6	45.1	25648.6	1
	–	–	–	28.41	48.0	38.1	35.8	1
	–	–	–	26.90	85.2	36.1	63.6	1
	–	–	–	25.36	141.5	34.0	105.6	1
	–	–	–	19.27	6063.0	25.8	4524.9	1
	–	–	–	17.08	217.9	22.9	162.6	1
	–	–	–	14.90	119.7	20.0	89.4	1
	–	–	–	12.87	80.9	17.2	60.4	1
	–	–	–	12.18	64.9	16.3	48.4	1
	–	–	–	12.00	23.9	16.1	17.8	1
	–	–	–	11.74	214.4	15.7	160.0	1
	–	–	–	10.85	23.7	14.5	17.6	1
090902B	19.3	6.8	1.82	21.72	332.2	61.3	117.7	1
	–	–	–	18.11	26.5	51.1	9.4	1
	–	–	–	15.40	45.9	43.5	16.3	1
	–	–	–	14.22	14.5	40.1	5.1	1
	–	–	–	12.66	42.7	35.7	15.1	1
	–	–	–	11.89	12.0	33.6	4.2	1

Notes. The unit of energy is GeV, T_{90} and arrival times are in seconds;

(^{a,d,e}) Observation Frame_{of}; (^{b,f,g}) Source Frame_{sf}; (^{a,ref}) <https://heasarc.gsfc.nasa.gov/cgi-bin/W3Browse/w3hdprods.pl>;
(^{c,ref}) <http://www.mpe.mpg.de/~jcg/grbgen.html>; (^h) Probability of the photon being associated with that GRB.

Table 4. The fitting parameters of the PL and BPL model of 7 GRBs which show a possible upturn in the afterglow spectra.

Name	PL model		BPL & BPL _{$\alpha-\beta=0.5$} model				
	Γ	TS	α	β	E_b	TS	ΔTS
190114C	2.37 ± 0.41	20.19	3.71 ± 0.89	1.39 ± 0.46	696 ± 283	27.92	7.73
	–	–	2.72 ± 0.37	$\alpha-0.5$	631 ± 202	22.93	2.74
171210A	2.33 ± 0.28	34.31	2.79 ± 0.49	1.48 ± 0.78	1368 ± 755	37.70	3.39
	–	–	2.51 ± 0.31	$\alpha-0.5$	1260 ± 424	36.18	1.87
150902A	2.52 ± 0.31	41.29	3.41 ± 0.55	1.55 ± 0.41	637 ± 222	49.28	7.99
	–	–	2.92 ± 0.45	$\alpha-0.5$	584 ± 274	44.39	3.10
131231A	1.72 ± 0.11	165.31	2.03 ± 0.58	1.32 ± 0.21	1586 ± 696	178.94	13.63
	–	–	1.93 ± 0.11	$\alpha-0.5$	1585 ± 783	178.60	13.29
130907A	1.79 ± 0.30	39.27	2.54 ± 0.56	1.08 ± 0.56	1741 ± 1007	42.89	3.62
	–	–	2.05 ± 0.28	$\alpha-0.5$	1712 ± 952	41.23	1.96
130427A	2.22 ± 0.10	611.14	2.38 ± 0.14	1.86 ± 0.28	1080 ± 545	615.00	3.86
	–	–	2.40 ± 0.15	$\alpha-0.5$	1080 ± 361	614.97	3.83
090902B	1.86 ± 0.11	458.53	2.31 ± 0.16	1.82 ± 0.14	664 ± 390	463.19	4.66
	–	–	2.40 ± 0.18	$\alpha-0.5$	584 ± 314	462.91	4.38

Notes. The unit of E_b is MeV. All spectral fits are made using 0.1–200 GeV data collected between $2 \times T_{90}$ and one day after. ΔTS is $TS_{BPL} - TS_{PL}$ and $TS_{BPL_{\alpha-\beta=0.5}} - TS_{PL}$.

Table 5. The fitting parameters of the PL and BPL model of 11 GRBs which do not show an upturn in the afterglow GeV spectra.

Name	PL model		BPL model				
	Γ	TS	α	β	E_b	TS	ΔTS
171022A	1.18 ± 0.73	13.03	2.33 ± 2.05	1.08 ± 0.46	1166 ± 623	13.35	0.32
171010A	2.07 ± 0.12	162.04	1.92 ± 0.24	2.31 ± 0.38	826 ± 407	164.15	2.11
160623A	1.85 ± 0.10	145.83	1.78 ± 0.23	1.91 ± 0.41	637 ± 222	145.66	-0.17
160310A	1.24 ± 0.64	10.02	1.81 ± 1.20	1.10 ± 0.69	1282 ± 629	10.18	0.16
140928A	1.14 ± 0.31	33.90	1.92 ± 0.71	0.84 ± 0.41	1999 ± 81	36.01	1.11
140810A	1.66 ± 0.20	59.29	0.01 ± 0.54	1.85 ± 0.29	559 ± 102	60.33	1.04
140416A	1.65 ± 0.40	16.52	1.38 ± 0.02	2.00 ± 0.64	516 ± 177	17.50	0.98
140206B	1.98 ± 0.11	177.00	2.08 ± 0.21	1.89 ± 0.21	917 ± 755	177.88	0.88
100414A	2.02 ± 0.14	98.58	0.73 ± 0.65	2.35 ± 0.26	310 ± 128	103.39	4.81
090926A	1.86 ± 0.08	176.70	1.87 ± 0.56	1.86 ± 0.22	999 ± 82	176.71	0.01
090510A	2.09 ± 0.07	381.12	2.00 ± 0.09	2.51 ± 0.36	2024 ± 186	383.79	2.67

Notes. The unit of E_b is MeV. All spectral fits are made using 0.1–200 GeV data collected between $2 \times T_{90}$ and one day after. $\Delta TS = TS_{BPL} - TS_{PL}$.

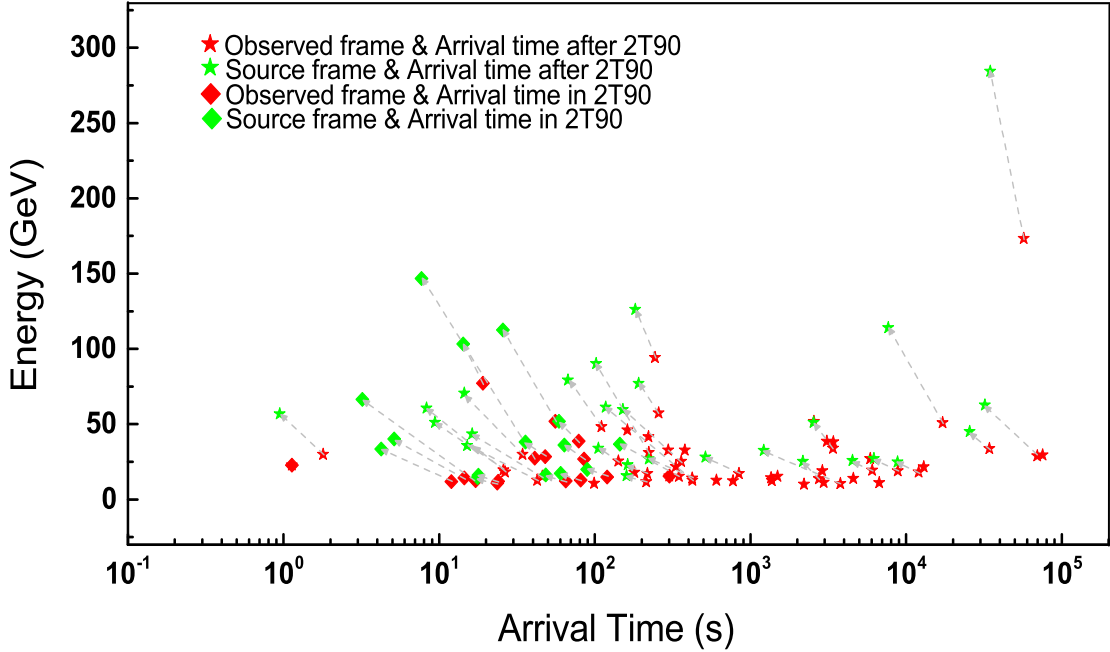


Fig. 1. The energy and arrival time of photons with detected energy ≥ 10 GeV from Fermi-LAT GRBs from burst onset to 1 day thereafter. Red symbols represent photons arrived within and after $2 \times T_{90}$, shown in \blacklozenge and \star , respectively. Photon energy and arrival time in the source frame are also shown (in green) if measured redshift are available. Dashed arrows connect the same photons in the source frame and the observer's frame.

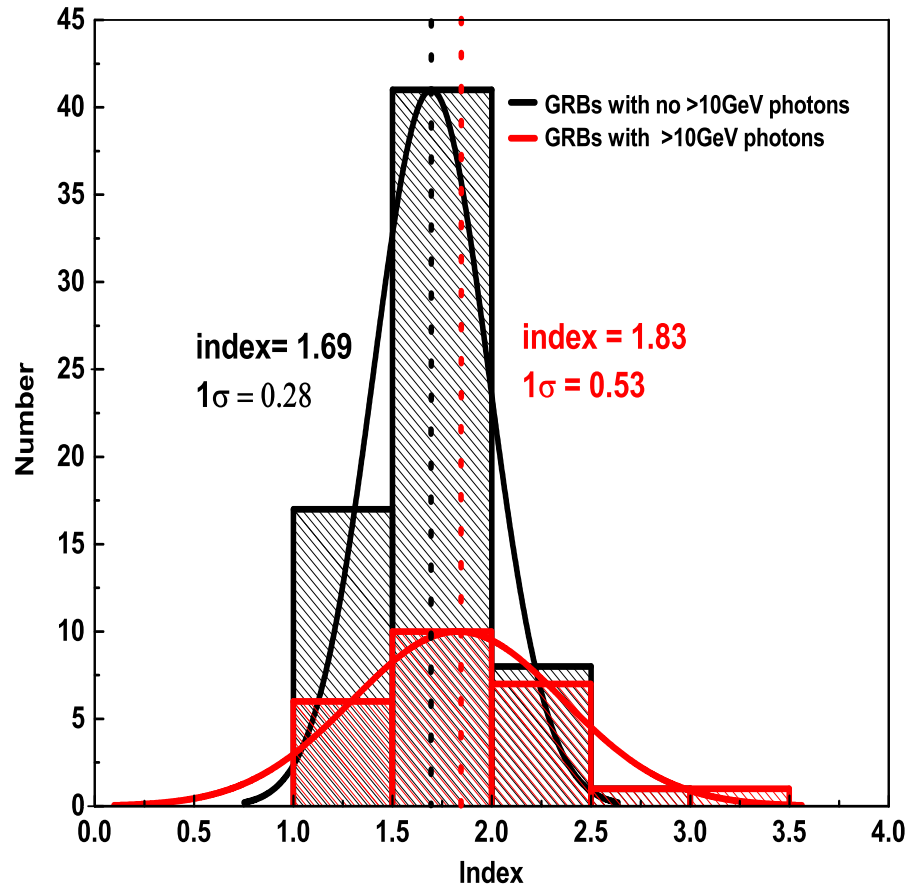


Fig. 2. The distribution of spectral index from 174 typical GRB afterglows (black) and the 25 GRBs with ≥ 10 GeV photons detected (red) respectively. The spectra of afterglows from $2 \times T_{90}$ to 1 day are fitted with the PL model in 0.1-200 GeV.

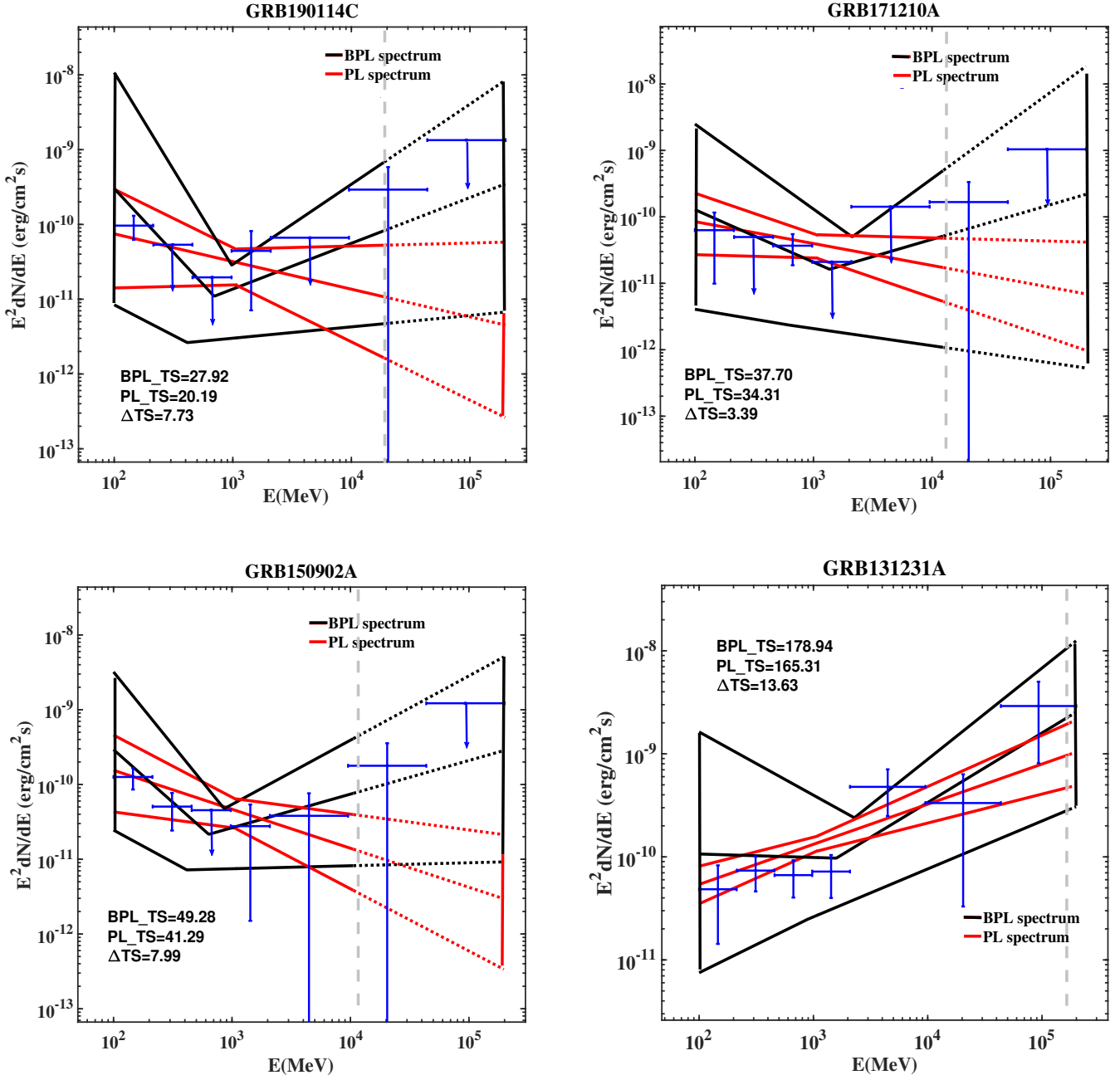


Fig. 3. The 0.1–200 GeV PL and BPL spectra of the 7 GRBs in the $E^2 dN/dE$ representation, using time range from the $2 \times T_{90}$ to one day thereafter. Red and black lines show the PL model fits and BPL model fits, respectively. All $\pm 1\sigma$ error contours are propagated from errors on the fit parameters. The vertical, dashed lines indicate the energy of the most energetic photon detected. The spectra are extrapolated above the maximum photon energy to 200 GeV, and are shown as dotted lines. The blue data points are fits with a power-law in individual energy bands. The upper limits are calculated with assuming index = -3 (fixed).

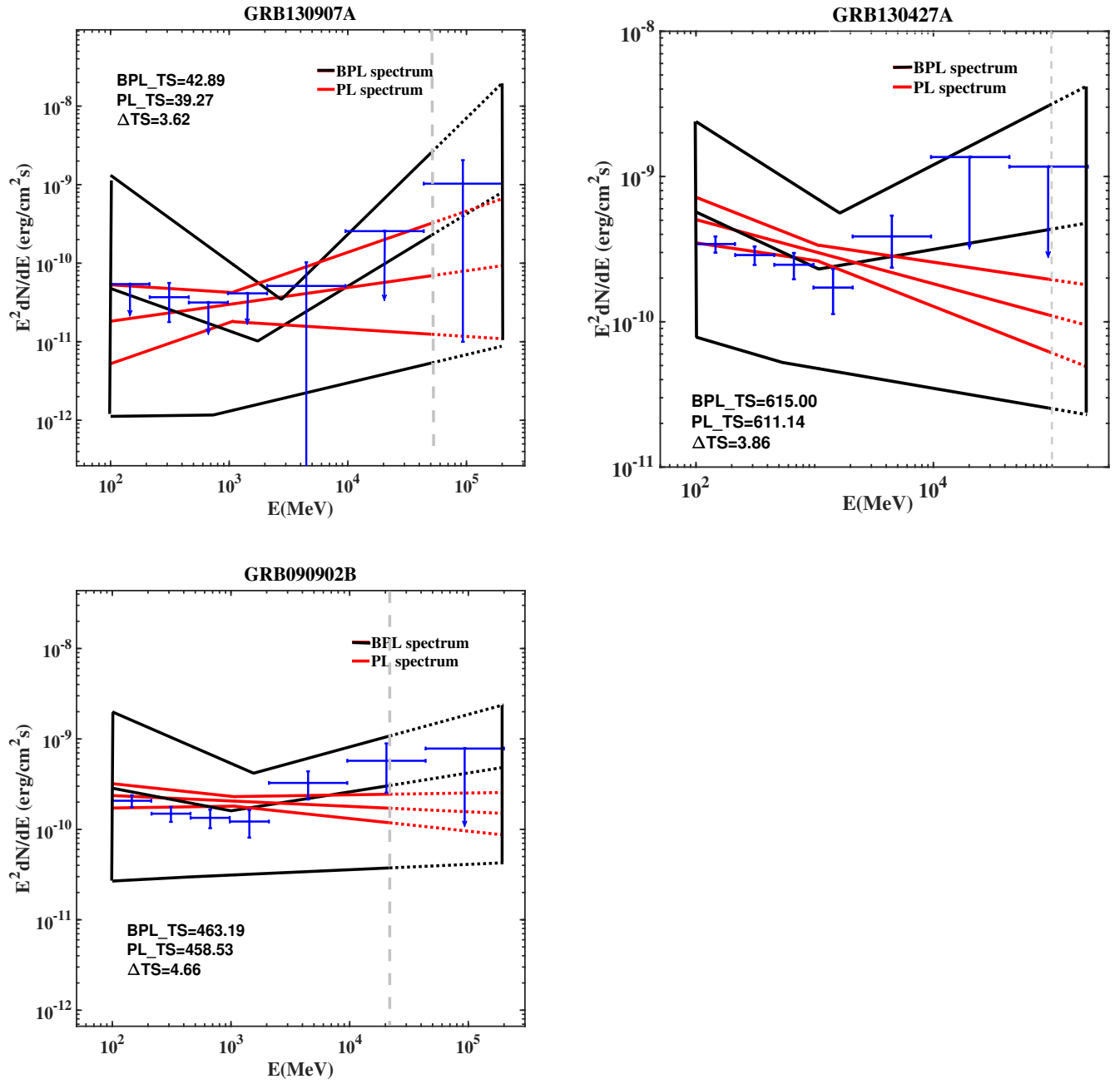


Fig. 3. continued from previous page

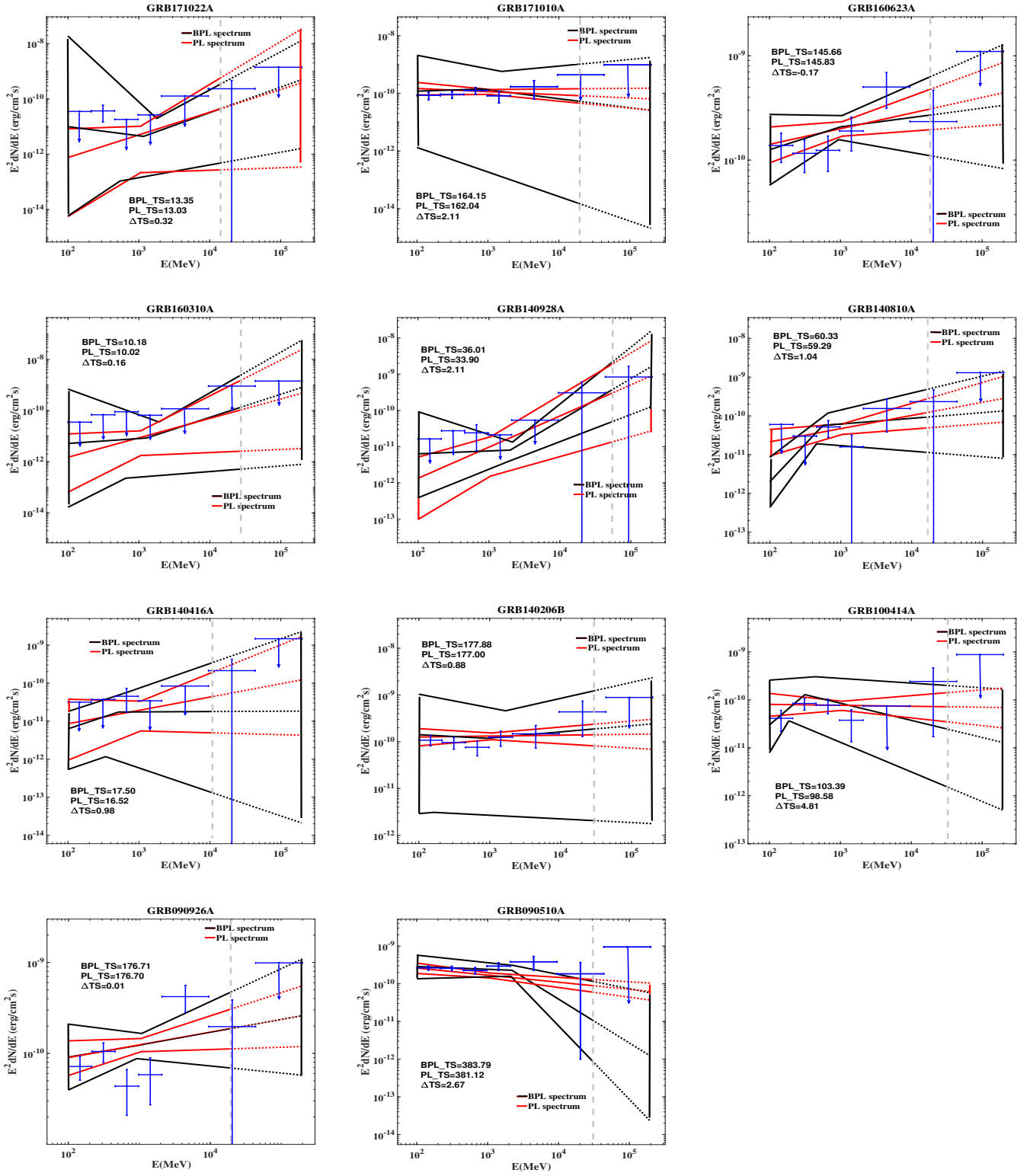


Fig. 4. The 0.1-200 GeV PL and BPL spectra of the remaining 11 GRBs in the $E^2 dN/dE$ representation, using time range from the $2 \times T_{90}$ to one day thereafter. Red and black lines show the PL model fits and BPL model fits, respectively. All the $\pm 1\sigma$ error contours are propagated from errors on the fit parameters. The vertical, dashed lines indicate the energy of the most energetic photon detected, and the spectra are extrapolated above the maximum photon energy to 200 GeV, and are shown as dotted lines. The blue data points are fits with a power-law in individual energy bands. The upper limits are calculated with assuming index = -3 (fixed).

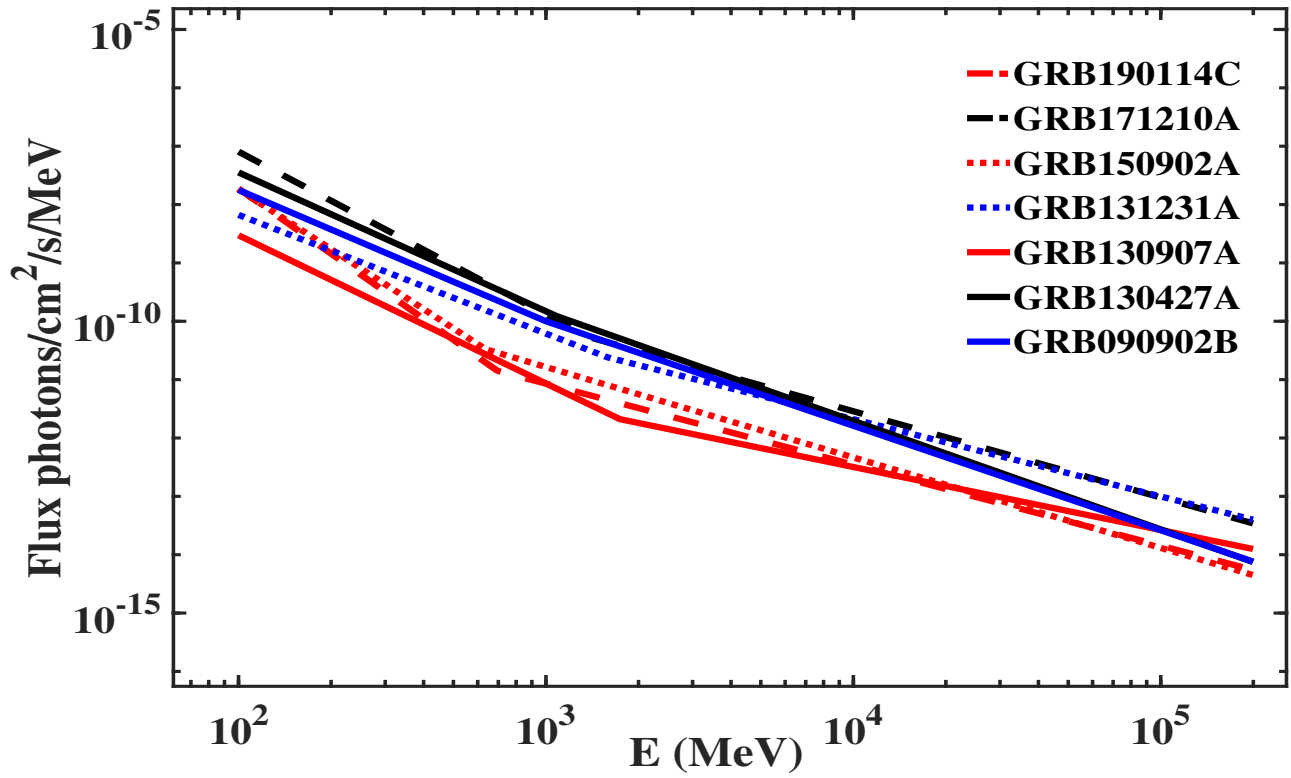
BPL model Of All Δ TS > 3 GRBs

Fig. 5. The best-fit broken power-law photon spectra of the 7 GRBs, which possibly reveal an upturn in the afterglow spectra and $\Delta\text{TS} = \text{TS}_{\text{BPL}} - \text{TS}_{\text{PL}} > 3$.

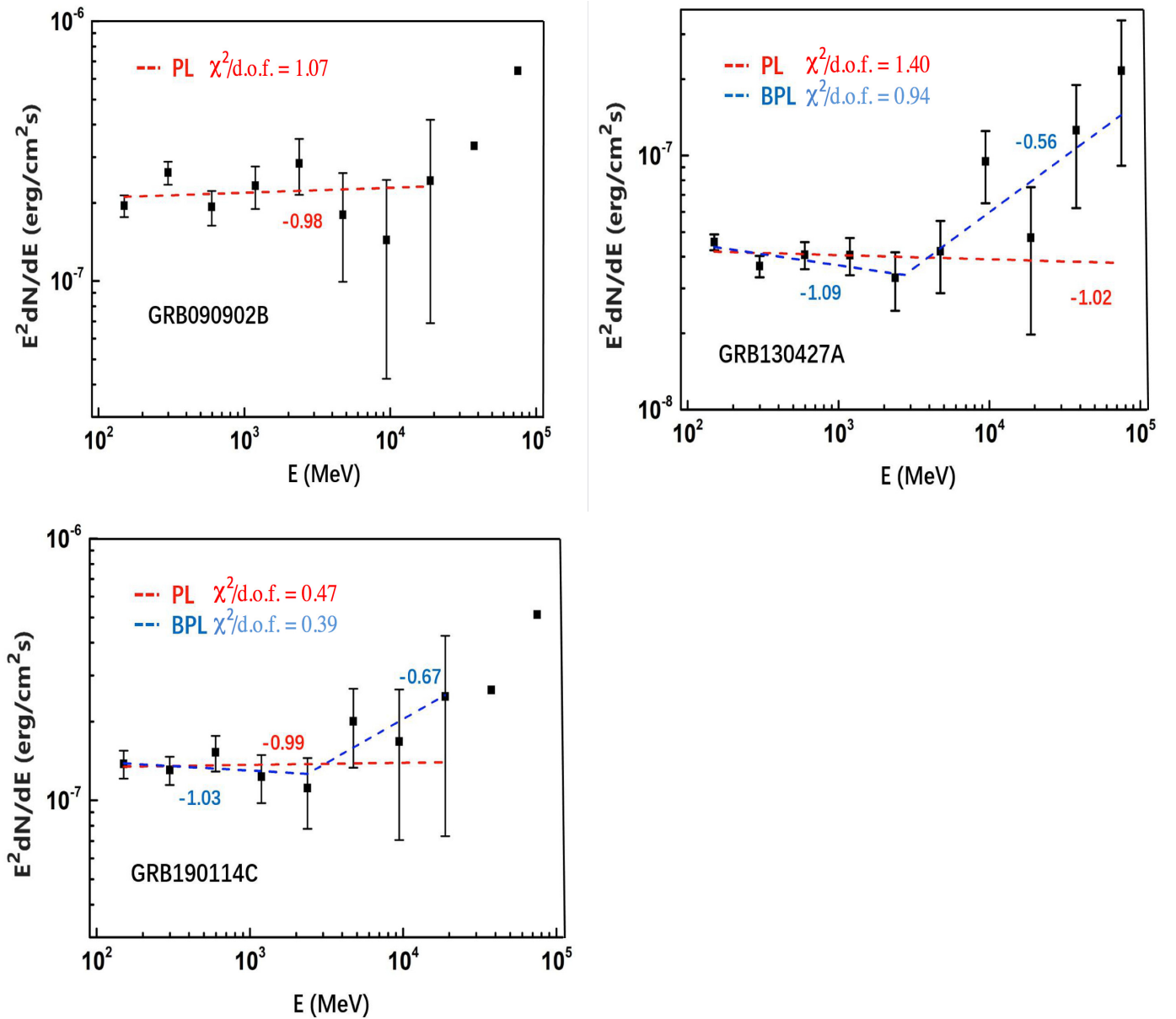


Fig. 6. The spectra F of GRB 090902B, GRB 130427A and GRB 190114C in the time interval T_0 to $2 \times T_{90}$. The single power-law fits are made starting from 100 MeV and up to where measurements can be fit. Data (squares) without error bars are upper limits, which are calculated assuming $\Gamma = -3$ (fixed). The dash lines are the fits of the data points with a PL (red) or BPL (blue) model. The numbers next to the model fits are the index of the spectra F in each energy interval.

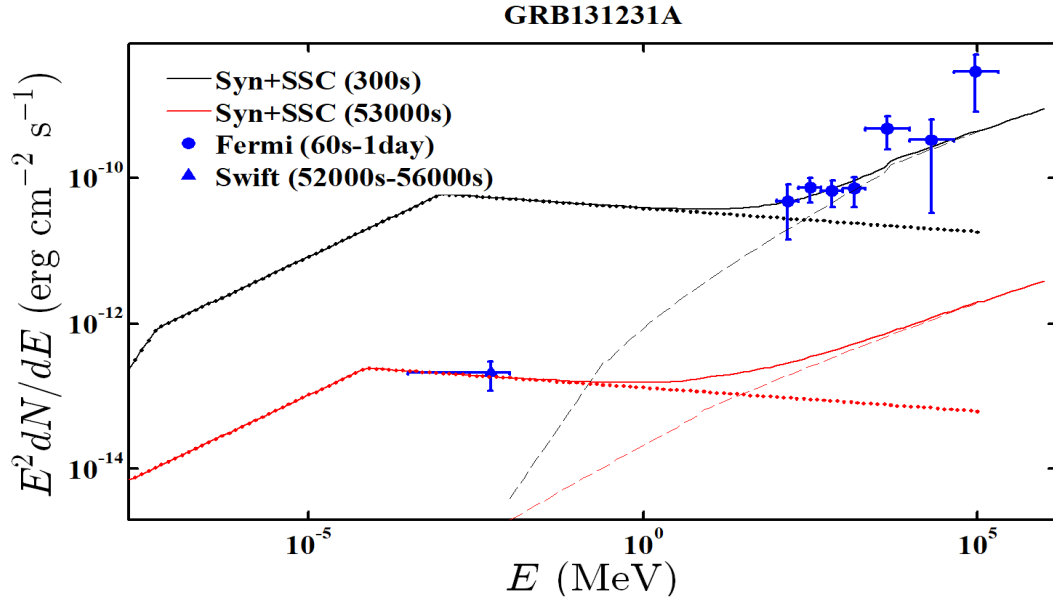


Fig. 7. Modelling the broadband spectra of GRB 131231A in the time intervals 60s-1day and 52000-56000s. Thick black curves represent the theoretical spectra of synchrotron plus SSC corresponding to slow cooling in the external forward shock scenario. Dotted line and dashed line represents the synchrotron and SSC component, respectively. The adopted parameters are $\epsilon_e=0.16$, $\epsilon_B=0.00001$, $p=2.13$, and $n=1 \text{ cm}^{-3}$.

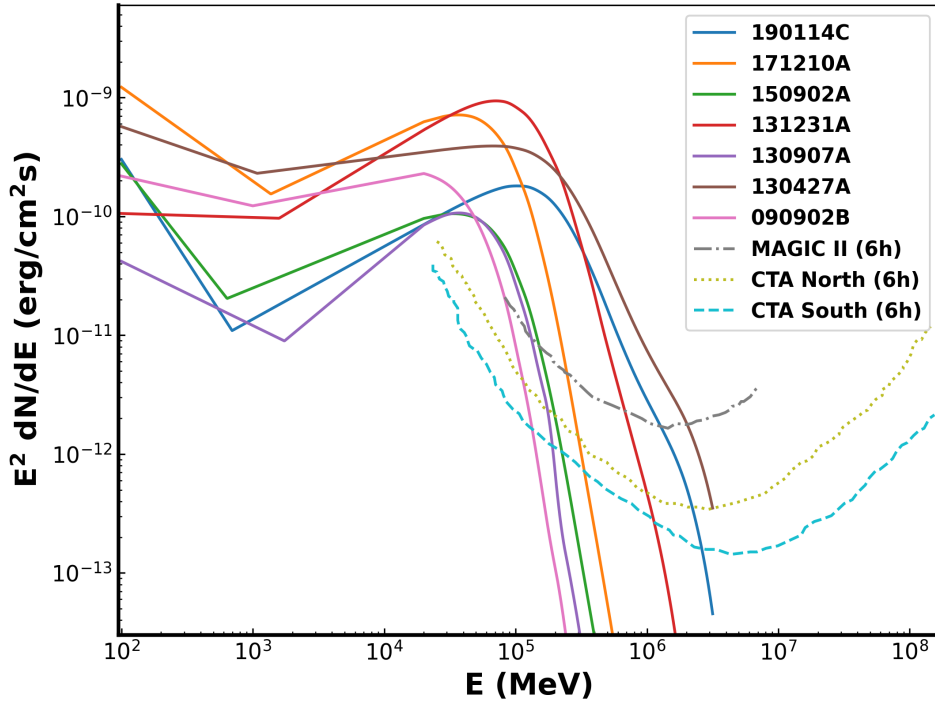


Fig. 8. The broken power-law energy spectra of the 7 GRBs and the 6-hour sensitivity of CTA and MAGIC. The time interval of the 7 GRBs are $2 \times T_{90}$ to 24h. We assume the high-energy index β of the intrinsic spectra extends up to 10 TeV.